Electronic Supplementary Information

Nitrogen-doped hollow carbon nanoflowers from preformed covalent triazine framework for metal-free bifunctional electrocatalysis

Yong Zheng[a], Shan Chen[a], Hui Song[a], Kai A. I. Zhang*[c], Chao Zhang*[a], and Tianxi Liu[a,b,d]

[a]*State Key Laboratory for Modification of Chemical Fibers and Polymer Materials, College of Materials Science and Engineering, Innovation Center for Textile Science and Technology, Donghua University, Shanghai 201620, P. R. China*

[b]*Key Laboratory of Synthetic and Biological Colloids, Ministry of Education, School of Chemical and Material Engineering, Jiangnan University, Wuxi 214122, P. R. China*

[c]*Department of Materials Science, Fudan University, Shanghai 200433, P. R. China*

[d]*Key Laboratory of Materials Processing and Mold (Zhengzhou University), Ministry of Education, Zhengzhou 450002, P. R. China*

1. Experimental section

1.1 Materials

Melamine, cyanuric acid and ethanol (99.5%) were purchased from Sinopharm Chemical Regent. Cyanuric chloride (99%), piperazine (99.5%), potassium hydroxide (KOH ≥ 90%) were purchased from Sigma-Aldrich. Tetrahydrofuran (THF, AR), dimethyl sulfoxide (DMSO, AR) and triethylamine (TEA, AR) were supplied from Aladdin and distilled before use. Deionized water (DI water) was used throughout the experiments. All the chemicals were used as received without further purification unless specified.

1.2 Synthesis of Melamine cyanurate (MCA)

Typically, melamine (0.50 g) and cyanuric acid (0.51 g) were dissolved in 20 mL and 10 mL of dimethyl sulfoxide (DMSO), respectively. After complete dissolution by sonication, the as-prepared solutions were mixed quickly and stirred again for 15 min. The MCA was separated by vacuum filtration, washed with ethanol, and dried overnight at 60 °C under vacuum.

1.3 Synthesis of the CTF-PP@MCA-X

The CTF-PP@MCA composites were prepared by in-situ polycondensation of the cyanuric chloride and piperazine on the surface of MCA using TEA as acid-binding agent. First, 1.0 g of MCA was dispersed in 25 mL of THF, then designed amounts of cyanuric chloride, and then piperazine were added into the suspension. After 10 mins, 2 mL of TEA was added and the following reaction was carried out at three temperature stages, namely, at ~ 0 ºC for 2 h, room temperature for 4 h and 80 ºC overnight. The precipitates, denoted as CTF-PP@MCA-X were filtered, washed with excess THF, ethanol and DI water for three times, respectively, and then dried in vacuum at 60 °C for 12 h. The CTF-PP@MCA-1, CTF-PP@MCA-2, and CTF-PP@MCA-3 represent the samples with 150, 300, and 600 mg of the cyanuric chloride monomer, respectively.

1.4 Synthesis of N-HCNF-X-T

The CTF-PP@MCA-X nanocomposites were transferred into a covered crucible and pyrolyzed at T ºC (T = 800, 900, 1000, 1100) for 2 h with a heating rate of 5 °C min^{-1} under a continuous flow of nitrogen to obtain N-HCNF-X-T. As a control experiment, the CTF-PP was used as precursor by following the same carbonization procedures.

1.5 Characterization

The morphologies of the powder products were studied by field-emission scanning electron microscopy (FESEM, JEOL JSM-7001F) and transmission electron microscopy (TEM, JEOL JEM-2100). The crystalline phases of the obtained products were characterized by X-ray diffractometer on a Bruker D8 Advance. The FT-IR spectra were measured with a Nicolet Impact 410 Fourier transform infrared spectrometer. Raman measurements were performed using a Renishaw inVia with a laser wavelength of 633 nm. XPS analysis was conducted on a Karatos Axis ULTRA X-ray photoelectron spectrometer. The nitrogen adsorption/desorption isotherms were collected at the temperature of liquid nitrogen (77 K) utilizing a QUADRASORB SI automated surface area and pore size analyzer (Quantachrome Corporation). The specific surface area was calculated from the adsorption data according to the Brunauer-Emmett-Teller (BET) method. The pore size distribution was derived with a nonlocal density functional theory (DFT) on the desorption branch. Prior to the measurements, samples were outgassed at 150 °C in vacuum for 24 h. TGA was performed on TG 209 F1 from room temperature to 1000 °C in air with a heating rate of 10 °C min^{-1}.

1.6 Electrochemical measurements

The both ORR and HER electrochemical performance of the as-prepared catalysts was analyzed on a CHI 660D electrochemical workstation (Shanghai, Chenhua Instruments). A standard three-electrode system was applied, using an Ag/AgCl electrode as the reference electrode, a graphite rod as the counter electrode, and a glassy carbon (GC) disk with an area of 0.196 cm^2 was used as the working electrode. The catalyst ink was prepared by adding 5 mg of the catalyst powder into a mixed solution of 95 μL of Nafion solution (5 wt%, Sigma Aldrich) and 350 μL of ethanol under sonication for 20 min. Then 5 μL of the catalyst ink was cast onto the grassy carbon electrode and dried at room temperature. For comparison, commercial Pt/C (20 wt%, Johnson Matthey Corp.) with a similar loading was also performed.

ORR measurement: Catalytic activity of a catalyst was measured by cyclic voltammetry (CV) at a scan rate of 50 mV s^{-1} and linear sweep voltammetry (LSV) at different rotation speeds of 800, 1200, 1600, 2000 and 2400 rpm at a scan rate of 10 mV s^{-1} on a rotating disk electrode (RDE, Pine AFMSRCE 2762). All potentials are normalized to a reference hydrogen electrode (RHE) using the following equation (1):

$$E\ (\text{vs. RHE}) = E\ (\text{vs. Ag/AgCl}) + 0.197 + 0.0592 \times \text{pH} \quad (1)$$

The LSV curves were carried out in a 0.1 M O_2-saturated KOH electrolyte with a potential range from 0.2 to 1.2 V (vs. RHE). Before the RDE test, the electrodes were scanned for 50 CV cycles with a scan rate of 100 mV s^{-1} in a 0.1 M O_2-saturated KOH electrolyte to activate the catalyst. The long-term stability of the catalyst was measured by conducting the chronoamperometric curves at 0.664 V vs. RHE at a rotation rate of 1600 rpm in a 0.1 M O_2-saturated KOH electrolyte. The methanol tolerance test was conducted by using the chronoamperometric response at 0.664 V vs. RHE in a 0.1 M O_2-saturated KOH with the addition of 1.0 M methanol. The electron transfer number (n) was carried out by a linear fitting using the Koutecky-Levich (K-L) equations (2), (3) and (4):

$$\frac{1}{J} = \frac{1}{J_L} + \frac{1}{J_K} = \frac{1}{B\omega^{1/2}} + \frac{1}{J_K} \qquad (2)$$

$$B = 0.62nFC_0(D_0)^{2/3}\upsilon^{-1/6} \qquad (3)$$

$$J_K = nFkC_0 \qquad (4)$$

where J is the actual measured current density, J_L is the diffusion limiting current density, J_K is the kinetic current density, ω is the angular rate of rotation, n is the electron transfer number, F is the Faraday constant (F = 96485 C mol^{-1}), C_0 is the bulk concentration of O_2 (C_0 = 0.0012 mol L^{-1}), D_0 is the diffusion coefficient of O_2 in KOH electrolyte (D_0 = 0.0000193 cm^2 s^{-1}), ν is the kinetic viscosity of the electrolyte (ν= 0.01 cm^2 s^{-1}), k is electron transfer rate constant. For (1), B is obtained from the slope of the K-L plot. Thus n is calculated from (2) when B is known, and the electron transfer number (n) can be calculated.

Rotating Ring-Disk Electrode (RRDE) Measurement: The disk electrode was scanned negatively at a rate of 5 mV s^{-1}, and the ring was held on a constant potential at 0.5 V versus Ag/AgCl. The H_2O_2 (%) and electron transfer number (n) can be calculated by equations (5) and (6):

$$H_2O_2(\%) = 200I_r/NI_d + I_r \qquad (5)$$

$$N = 4I_d/(I_d + I_r/N) \qquad (6)$$

where I_d is the disk current, I_r is the ring current. N is the ring collection efficiency of 0.37 (measured with the calibration of standard samples).[1] The calculation of electrochemically active surface area (ECSA) is based on the measured double layer capacitance of samples according to the previous report. A potential range of 1.04 to 1.14 V vs. Ag/AgCl was chosen

for the capacitance measurement where no faradic processes were observed at the scan rates of 10, 20, 30, 40, 50 mV s^{-1},respectively.[2]

HER measurement: A 0.5 M H_2SO_4 solution bubbled with N_2 was used as the electrolyte. The LSV curves were recorded at a scan rate of 5 mV s^{-1}. All the potentials in this study were iR corrected and converted to the RHE scale using the Nernst equation ($E_{RHE} = E_{Ag/AgCl} + 0.197 + 0.0592*$ pH).

Conductivity measurements: The conductivity of the N-HCNFs samples were measured using a 4-probe method (RTS-8, Guangzhou Four Probe Tech.) on wafers with a composition of 90 wt.% carbon-based materials and 10 wt.% polytetrafluoroethylene as a binder. The prepared composition was pressed, and disk-shaped well packed wafers were formed. The wafers were dried in an oven for 12 h. The thickness of the wafers was measured by a spring micrometer.

Assembly of a primary Zn-Air battery: The discharge behavior of the Zn-air battery was measured with a potentiostat. A polypropylene membrane (Celgard 5550) was used as the separator and a carbon cloth was used as the current collector. The catalyst ink was sprayed onto the carbon paper by using a gunjet with a loading of 1 mg cm^{-2}, followed by drying at 60°C for 30 min. A Zn plate was polished and used as the anode. The air electrode and Zn plate assembled into a battery with the cathode exposed to oxygen bubbles, and a 6 M KOH aqueous solution containing 0.2 M zinc acetate was utilized as the electrolyte. The commercial Pt/C catalyst (20 wt%) with the same mass loading was also coated on carbon paper and assembled into a Zn-air battery for comparison.

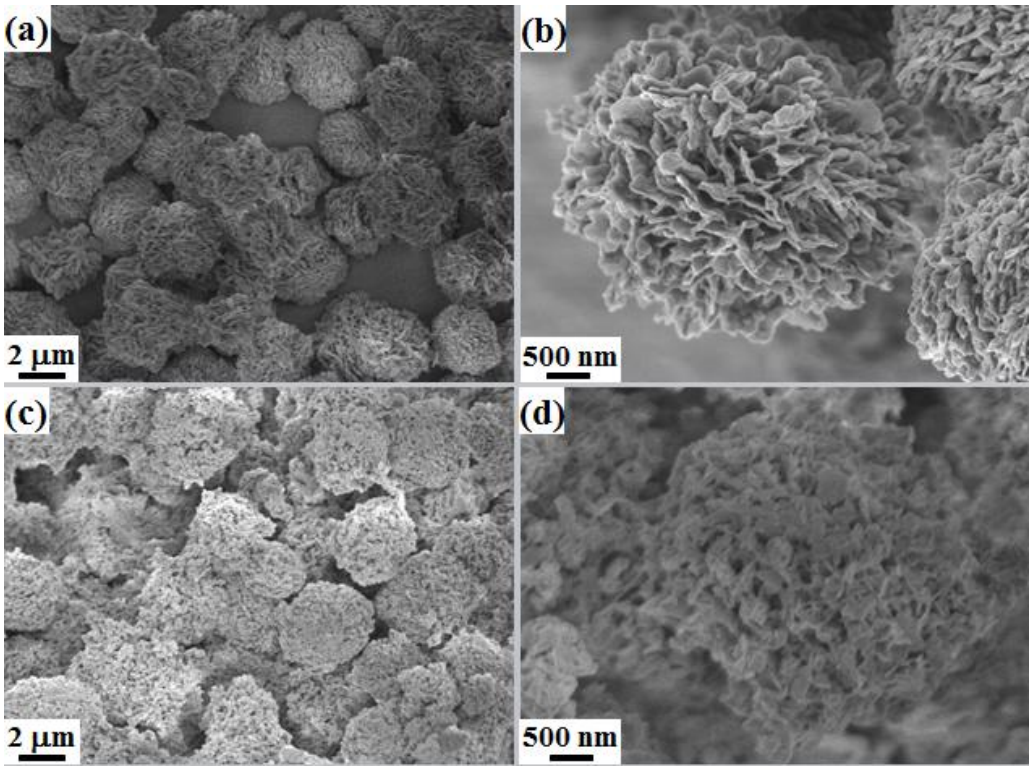

Fig. S1. SEM images of (a-b) CTF-PP@MCA-1, (c-d) CTF-PP@MCA-3.

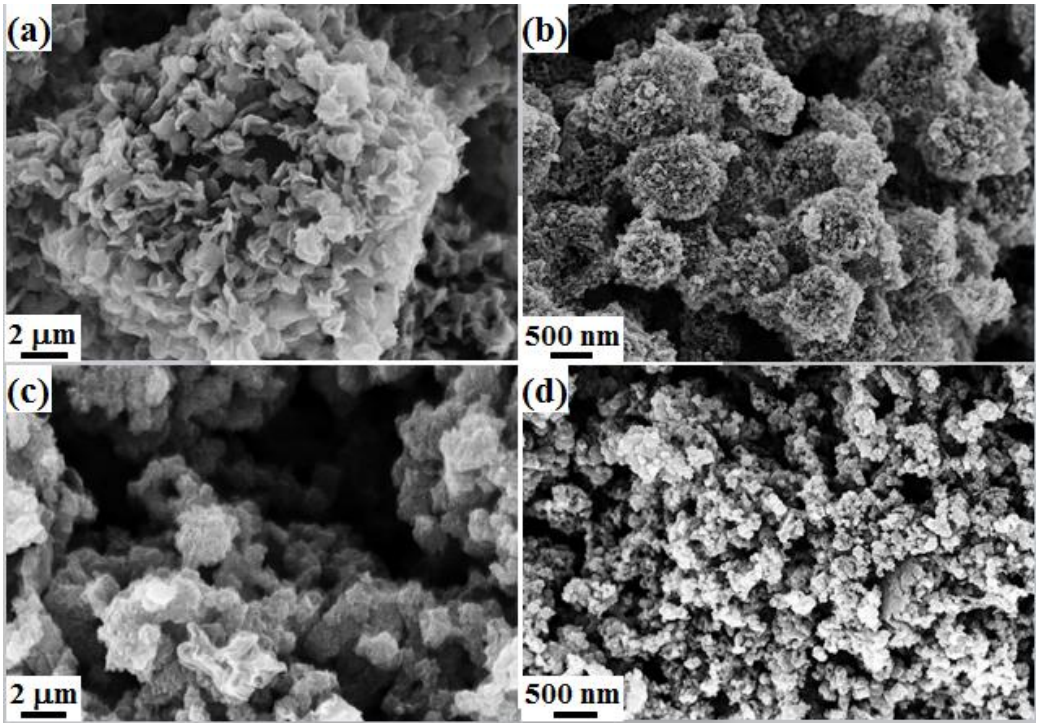

Fig. S2. SEM images of (a-b) N-HCNF-2-900, (c-d) N-HCNF-2-1100.

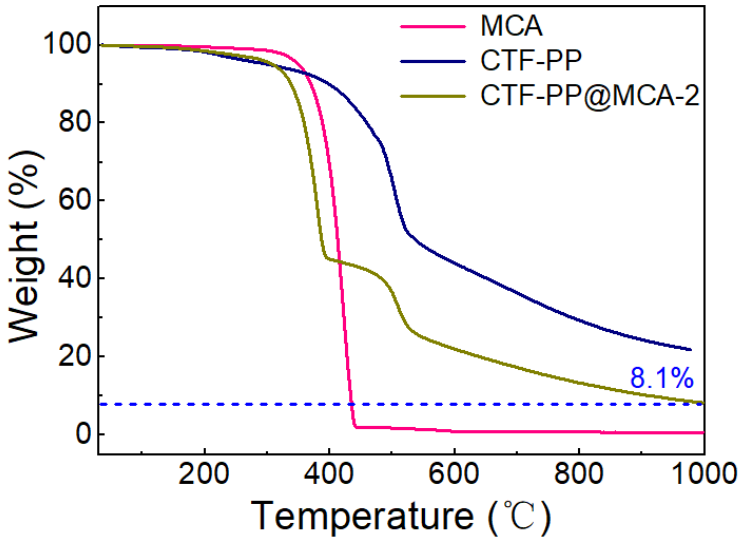

Fig. S3. TGA curves of corresponding samples.

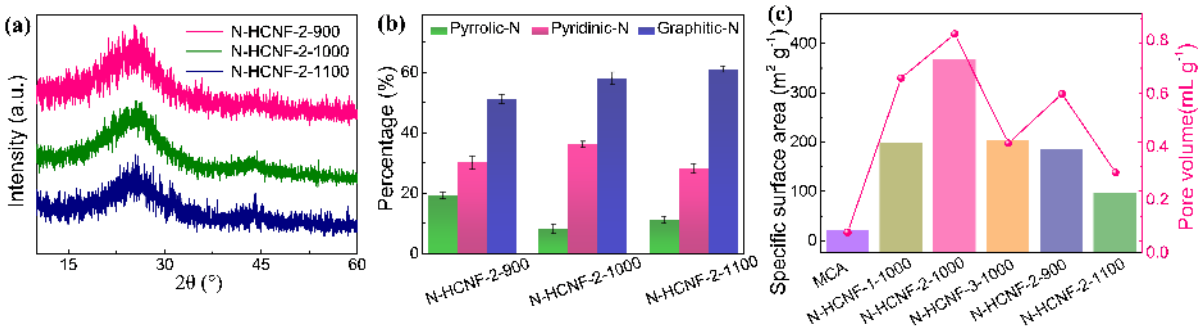

Fig. S4 (a) XRD patterns and (b) Percentage of the N types of the corresponding samples, (c) The SSA and pore volume of different samples.

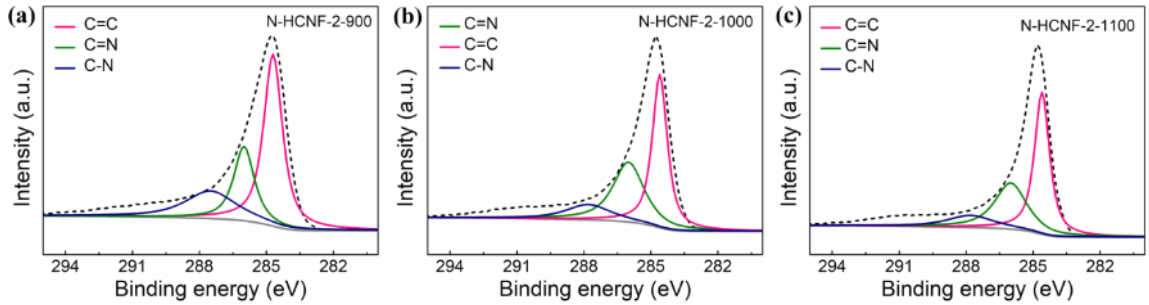

Fig. S5. High-resolution C 1s XPS spectra of (a) N-HCNF-2-900, (b) N-HCNF-2-1000 and (c) N-HCNF-2-1100.

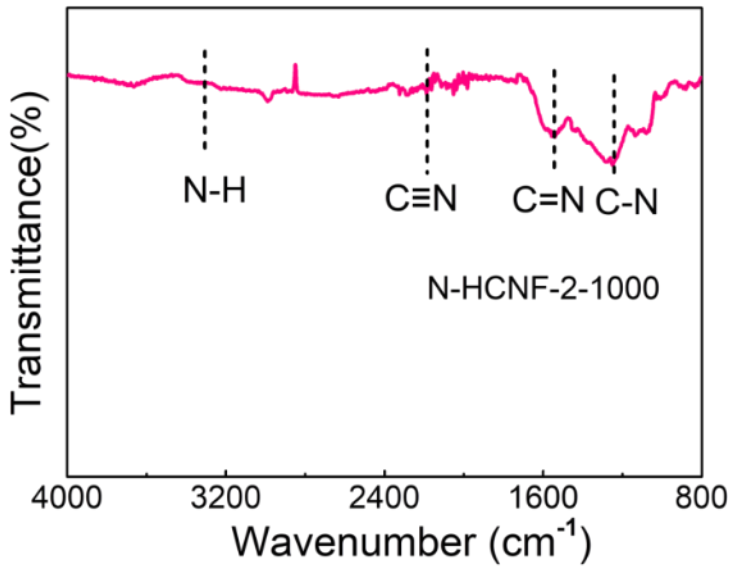

Fig. S6. FT-IR spectra of N-HCNF-2-1000.

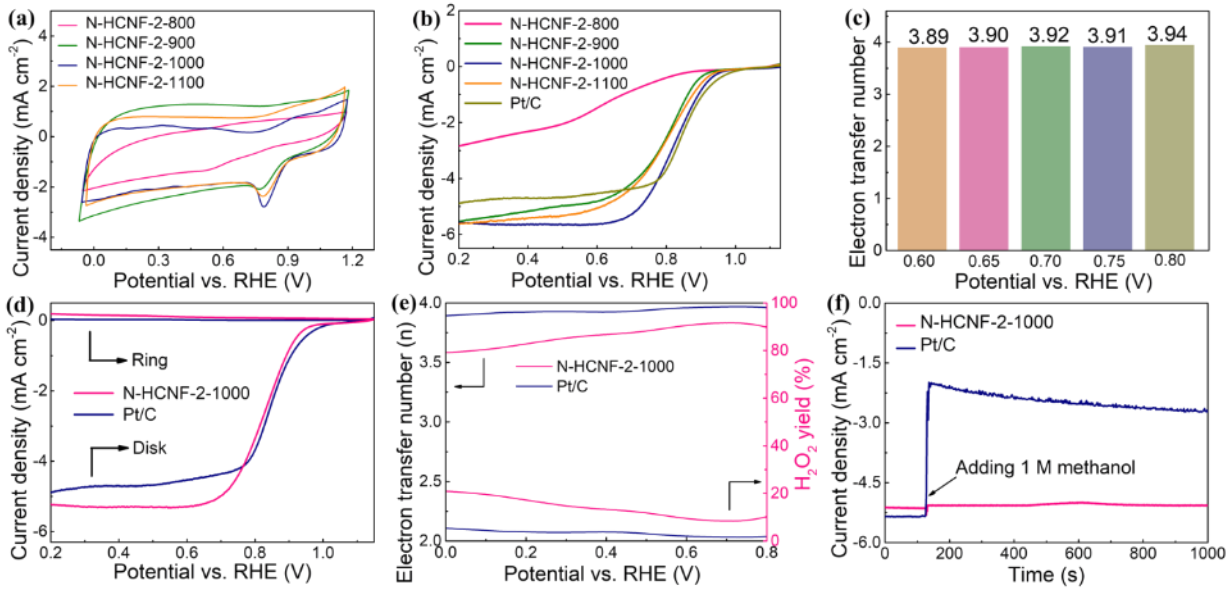

Fig. S7. ORR performance: (a) CV curves of N-HCNF-2-800, N-HCNF-2-900, N-HCNF-2-1000 and N-HCNF-2-1100, (b) LSV curves of the corresponding samples. (c) The N of N-HCNF-2-1000 at 0.6-0.8 V, (d) Ring current and disk current of the N-HCNF-2-1000 and Pt/C, (e) Electron transfer number and H_2O_2 yield of the N-HCNF-2-1000 and Pt/C, (f) Chronoamperometric responses of N-HCNF-2-1000 and Pt/C in O_2-saturated 0.1 M KOH adding 1 M methanol.

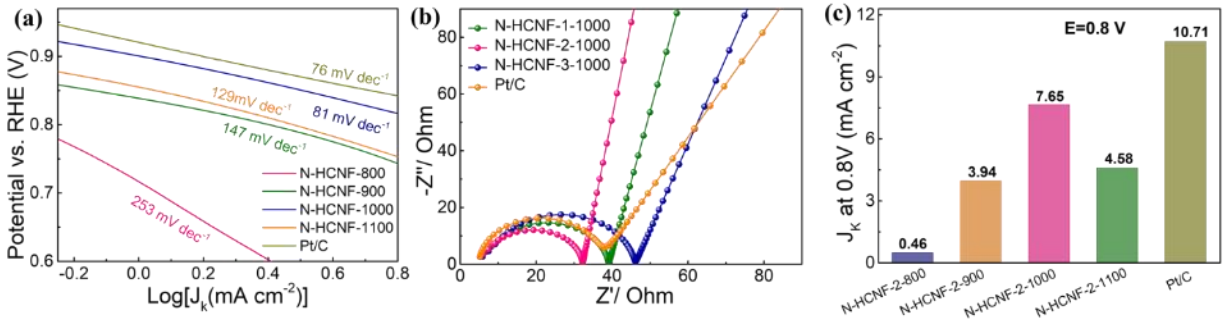

Fig. S8. (a) The Tafel curve of corresponding samples. (b) EIS patterns of corresponding samples. (c) The J_k of the corresponding samples.

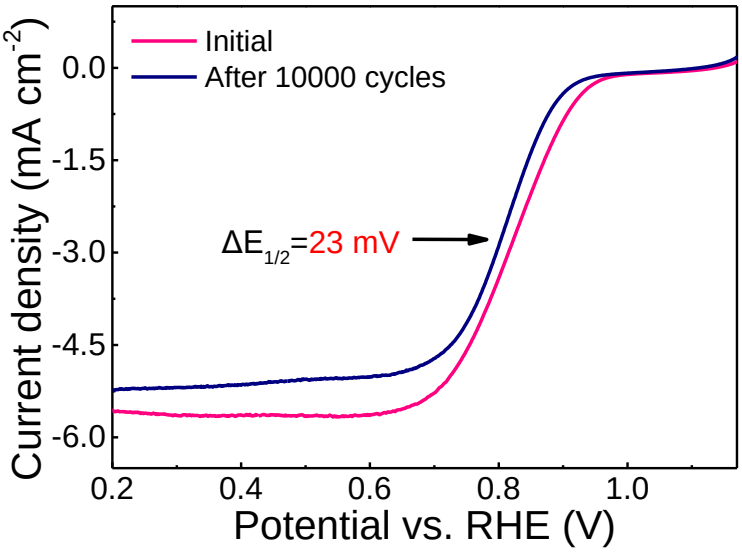

Fig. S9 The LSV curves of N-HCNF-2-1000 before and after 10000 cycles of CV tests.

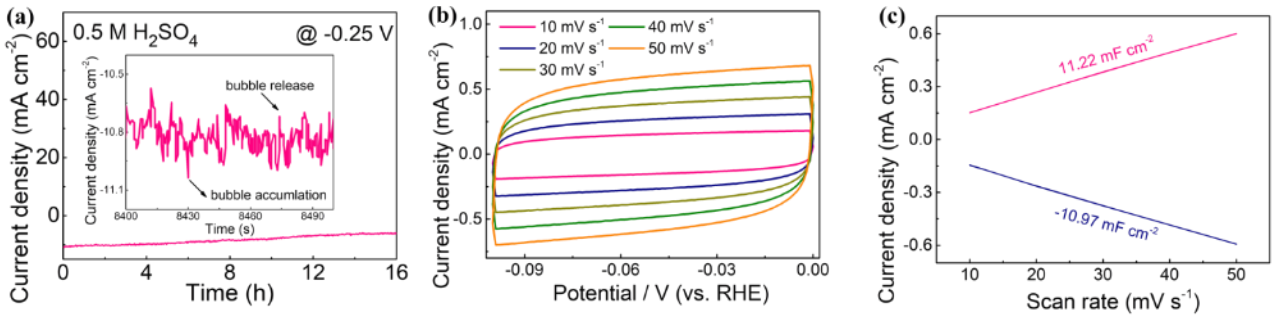

Fig. S10. (a) I-t plots of the N-HCNF-2-1000. (b) CV plots of N-HCNF-2-1000. (c) The tested capacitive currents plotted as a function of the rates.

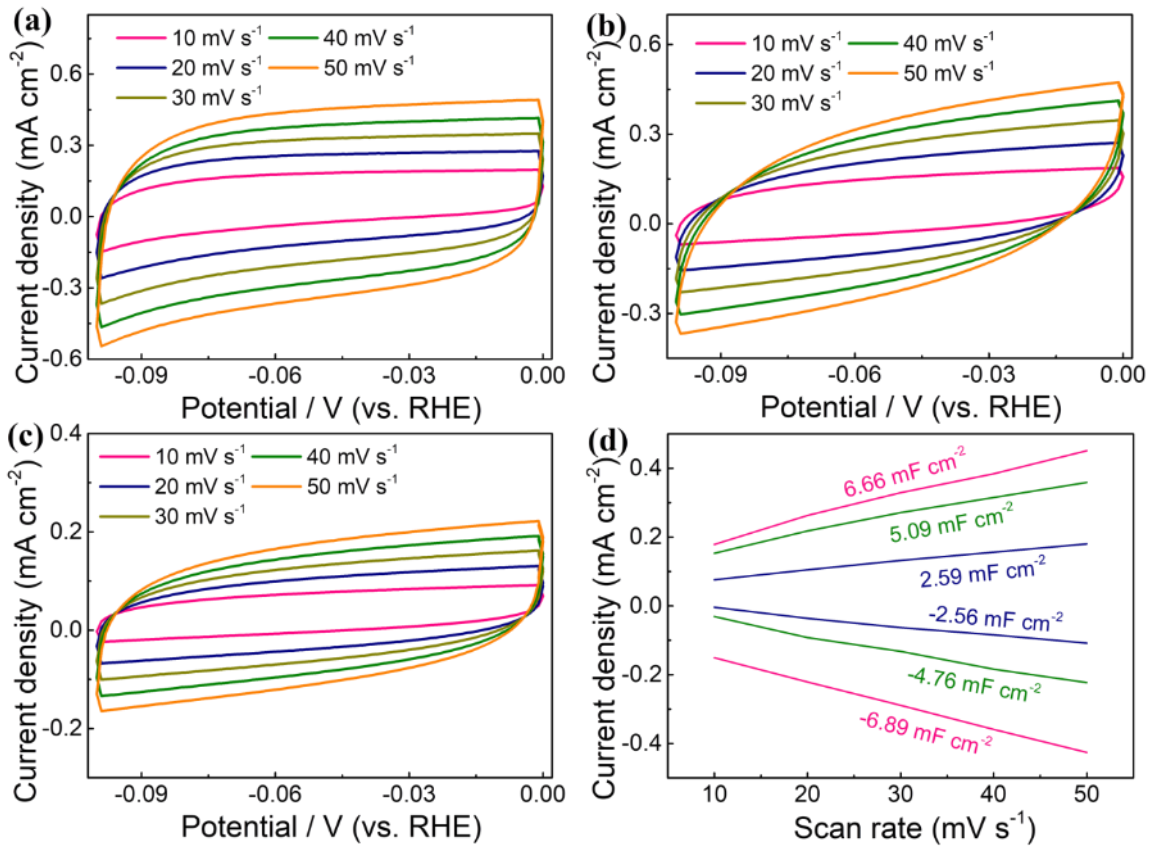

Fig. S11. CV plots of (a) N-HCNF-2-1100, (b) N-HCNF-2-900, (c) N-HCNF-2-800 at different scan rates. (d) The tested capacitive currents plotted as a function of the rates.

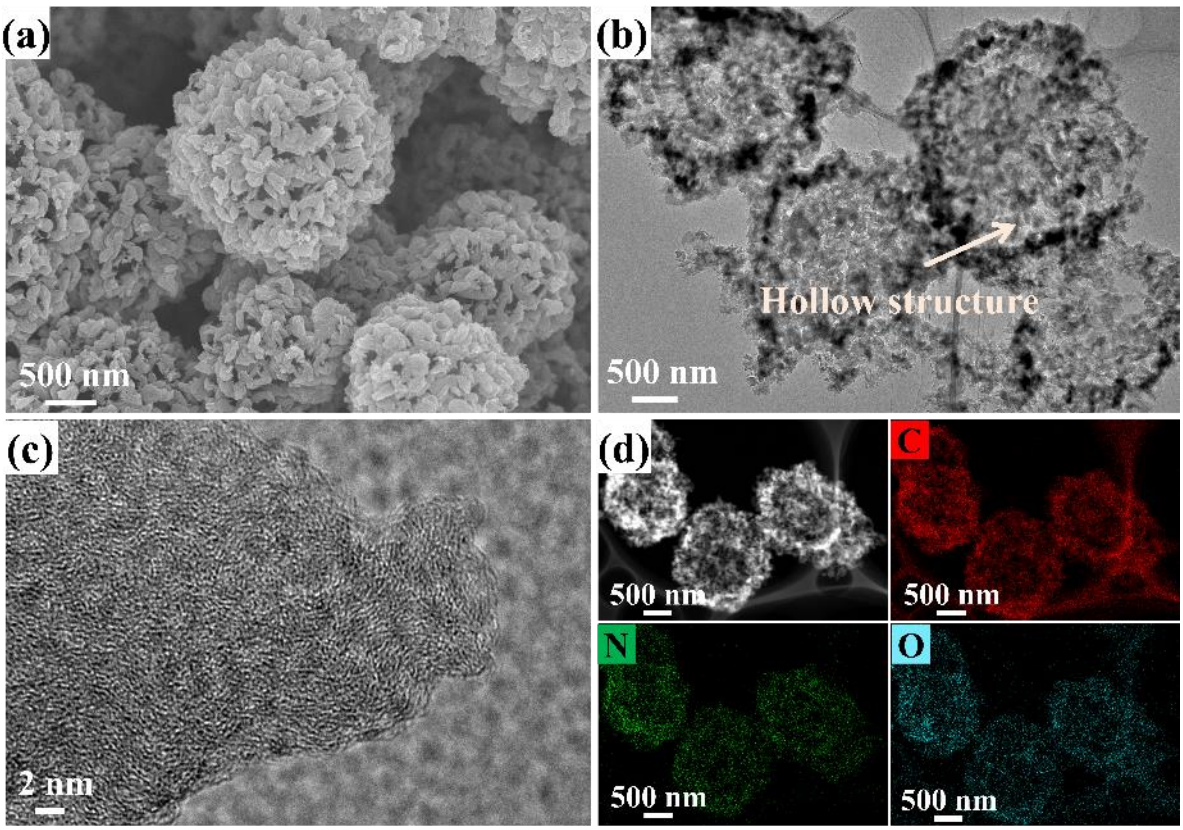

Fig. S12 (a) SEM images, (b) TEM images, (c) HRTEM images, (d) TEM image and corresponding elemental mappings of N-HCNF-2-1000 after the stability test, indicating C, N and O elements are still uniform distributed in N-HCNF-2-1000 after the stability test.

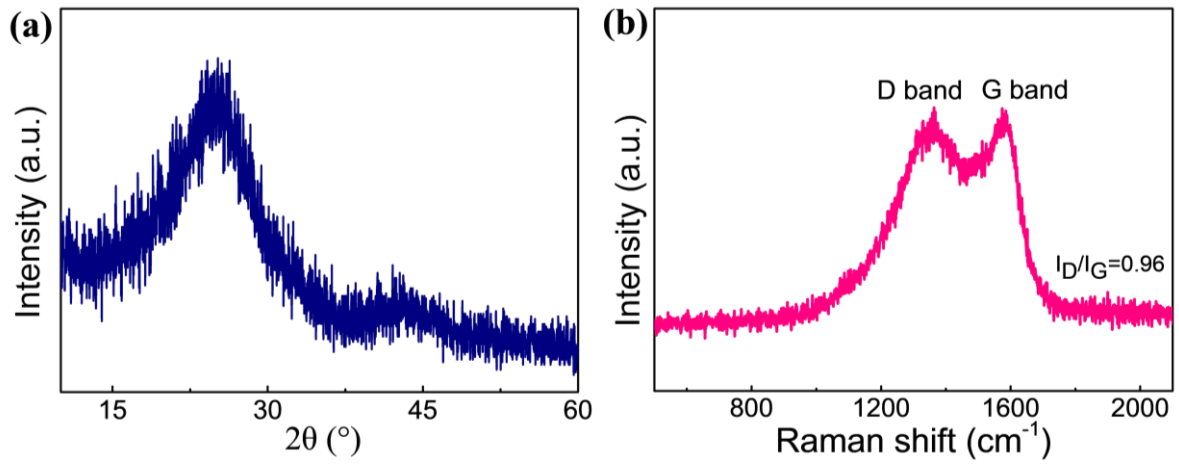

Fig. S13 (a)The XRD patterns and (b) Raman spectra of N-HCNF-2-1000 after the stability test.

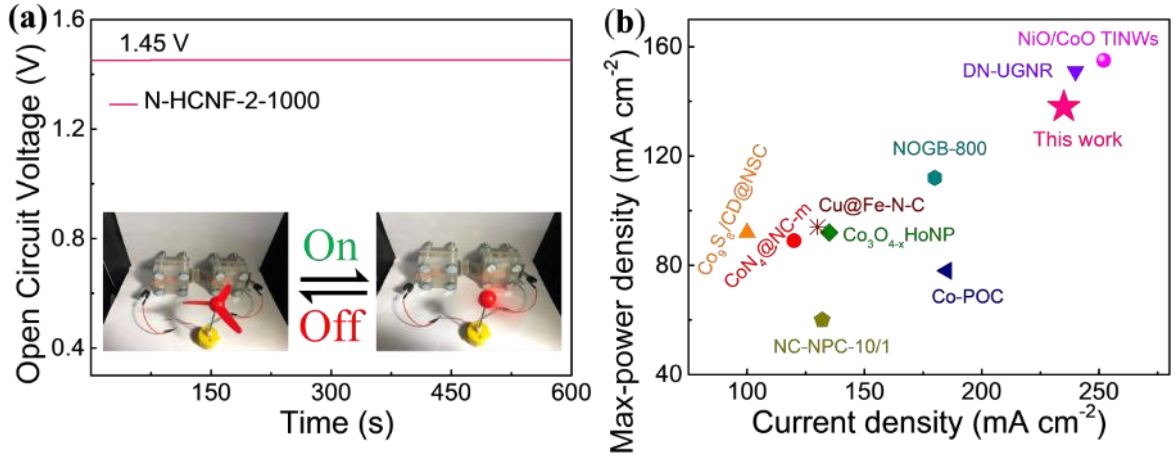

Fig. S14. (a) Open circuit voltage plots of the N-HCNF-2-1000, (b) Comparison of max-power density of N-HCNF-2-1000 with the different electrocatalysts in the literature.

Table S1. Electrical conductivity of the N-HCNFs as measured by 4-probe method.

Sample	Conductivity (k) (S/m)	Resistivity (q) (ohm m)
N-HCNF-2-900	72.8	1.4 E-02
N-HCNF-2-1000	155.4	6.4 E-03
N-HCNF-2-1100	208.5	4.8 E-03

Table S2. Summary of ORR performance of N-HCNF-2-1000 and other heteroatom-doped metal-free carbon catalysts in the literature.

Sample	$E_{1/2}$ [V] (vs RHE)	E_0 [V] (vs RHE)	Electron transfer number	Refs.
VA-NCNT	0.83	0.97	3.90	3
Carbon-L	0.70	0.86	3.68	4
N,S,O-OMC	0.73	0.85	3.50	5
N,S-CN	0.75	0.90	3.98	6
NCNC 700/900	0.78	0.87	3.27	7
N-CNF aerogel	0.80	0.91	3.96	8
WHC-700	0.85	0.98	3.64-3.93	9
NPMC-1000	0.94	0.85	~4.00	10
P-G	0.91	0.74	3.82-3.85	11
NOPHC10-900	0.90	0.77	3.64-3.74	12
NCN-1000-5	0.95	0.82	3.92	13
B-rGO	0.77	0.46	3.59	14
NS/C-950	1.01	0.85	3.97	15
mesoCF	0.98	0.81	3.4~3.8	16
NSPC-0.2-900	0.93	0.83	3.2	17
N,F-Carbon1000	0.97	0.84	3.92-3.98	18
C-COP-4	-	0.78	3.90	19
N-HCNF-2-1000	**0.84**	**1.01**	**3.89~3.94**	**This Work**

References

1. Y. Su, Z. Yao, F. Zhang, H. Wang, Z. Mics, E. Cánovas, M. Bonn, X. Zhuang and X. Feng, *Adv. Funct. Mater.*, 2016, **26**, 5893-5902.
2. C. C. L. McCrory, S. Jung, J. C. Peters and T. F. Jaramillo, *J. Am. Chem. Soc.*, 2013, **135**, 16977-16987.
3. K. Gong, F. Du, Z. Xia, M. Durstock and L. Dai, *Science*, 2009, **323**, 760-764.
4. P. Zhang, F. Sun, Z. Xiang, Z. Shen, J. Yun and D. Cao, *Energy Environ. Sci.*, 2014, **7**, 442-450.
5. J. Y. Cheon, J. H. Kim, J. H. Kim, K. C. Goddeti, J. Y. Park and S. H. Joo, *J. Am. Chem. Soc.*, 2014, **136**, 8875-8878.
6. K. Qu, Y. Zheng, S. Dai and S. Z. Qiao, *Nano Energy*, 2016, **19**, 373-381.
7. S. Chen, J. Bi, Y. Zhao, L. Yang, C. Zhang, Y. Ma, Q. Wu, X. Wang and Z. Hu, *Adv. Mater.*, 2012, **24**, 5593-5597, 5646.
8. H.-W. Liang, Z.-Y. Wu, L.-F. Chen, C. Li and S.-H. Yu, *Nano Energy*, 2015, **11**, 366-376.
9. X. Liu, Y. Zhou, W. Zhou, L. Li, S. Huang and S. Chen, *Nanoscale*, 2015, **7**, 6136-6142.
10. J. Zhang, Z. Zhao, Z. Xia and L. Dai, *Nat. Nanotechnol.*, 2015, **10**, 444.
11. L. Tao, Q. Wang, S. Dou, Z. Ma, J. Huo, S. Wang and L. Dai, *Chem. Commun.*, 2016, **52**, 2764-2767.
12. S. Huang, Y. Meng, Y. Cao, S. He, X. Li, S. Tong and M. Wu, *Appl. Catal., B*, 2019, **248**, 239-248.
13. H. Jiang, J. Gu, X. Zheng, M. Liu, X. Qiu, L. Wang, W. Li, Z. Chen, X. Ji and J. Li, *Energy Environ. Sci.*, 2019, **12**, 322-333.
14. Y. L. F. Musico, N. Kakati, M. F. M. Labata, J. D. Ocon and P.-Y. A. Chuang, *Mater. Chem. Phys.*, 2019, **236**, 121804.
15. X. Zhang, Y. Wang, Y. Du, M. Qing, F. Yu, Z. Q. Tian and P. K. Shen, *Electrochim. Acta*, 2019, **318**, 272-280.
16. J. Gao, Y. Wang, H. Wu, X. Liu, L. Wang, Q. Yu, A. Li, H. Wang, C. Song, Z. Gao, M. Peng, M. Zhang, N. Ma, J. Wang, W. Zhou, G. Wang, Z. Yin and D. Ma, *Angew. Chem. Int. Ed.*, 2019, **58**, 2-11.
17. L. Wang, K. Liang, L. Deng and Y.-N. Liu, *Appl. Catal., B*, 2019, **246**, 89-99.

18. Y. Lv, L. Yang and D. Cao, *ACS Appl. Mater. Interfaces*, 2017, **9**, 32859-32867.
19. Z. Xiang, D. Cao, L. Huang, J. Shui, M. Wang and L. Dai, *Adv. Mater.*, 2014, **26**, 3315-3320.